ELSEVIER

Journal of Alloys and Compounds 446–447 (2007) 681–686

Journal of ALLOYS AND COMPOUNDS

www.elsevier.com/locate/jallcom

Characterization of initial activation behavior for hydrogen storage alloys by acoustic emission technique

Hiroshi Inoue *, Ryosuke Tsuzuki, Shinji Nohara, Chiaki Iwakura

Department of Applied Chemistry, Graduate School of Engineering, Osaka Prefecture University, Sakai, Osaka 599-8531, Japan

Received 12 September 2006; received in revised form 14 December 2006; accepted 14 December 2006
Available online 23 December 2006

Abstract

We have monitored the physical processes linked to electrochemical processes *in situ* occurring at $MmNi_{3.6}Mn_{0.4}Al_{0.3}Co_{0.7}$ and $TiCr_{0.3}V_{1.8}Ni_{0.3}$ electrodes using an acoustic emission (AE) technique. The difference in initial activation behavior between both alloy electrodes was characterized by waveforms, power spectra and time history of the AE signals. In the first charging process, the cracking based on hydrogen absorption occurred intensively on the $MmNi_{3.6}Mn_{0.4}Al_{0.3}Co_{0.7}$ electrode in the first half, while the cracking on the $TiCr_{0.3}V_{1.8}Ni_{0.3}$ negative electrode occurred after hydrogen evolution. In the initial activation, the $MmNi_{3.6}Mn_{0.4}Al_{0.3}Co_{0.7}$ particles were broken down with many large and small cracks, while the $TiCr_{0.3}V_{1.8}Ni_{0.3}$ particles were not pulverized although a few cracks were observed.

Keywords: Hydrogen storage materials; Electrochemical reactions; Scanning electron microscopy; Acoustic emission

1. Introduction

Hydrogen absorption into hydrogen storage alloys causes the cracking of the alloy particles as a result of lattice expansion. Appearance of fresh alloy surface accelerates the hydrogen absorption. At hydrogen storage alloy negative electrodes used in nickel–metal hydride (Ni–MH) batteries, the hydrogen absorption occurs in charging. In this case, the cracking of alloy particles leads to the increase in discharge capacity. The discharge capacity increases with repeating charge–discharge cycles and finally reaches a constant value. In this way, most of hydrogen storage alloy electrodes need initial activation in which charge–discharge cycles are repeated until discharge capacity reaches a constant value [1]. The number of charge–discharge cycles required for the initial activation depends on hydrogen storage alloys used. For example, AB_5-type alloy electrodes have a constant discharge capacity in several charge–discharge cycles while AB_2-type Laves-phase alloy electrodes need several dozen cycles.

The effect of the initial activation has been inferred by *ex situ* analyses like scanning electron microscopy after discharge capacity reached a constant value. Notten et al. succeeded in *in situ* monitoring of lattice constants of hydrogen storage alloys during charging by X-ray diffractometry, and clarified the relationship between the lattice volume and the amount of absorbed hydrogen in detail [2]. Unfortunately, there have been quite a few *in situ* methods for analyzing the initial activation behavior.

The acoustic emission (AE) method is a nondestructive and sensitive technique for detecting elastic waves generated by the cracking of materials. In addition, the AE method can be used for real time *in situ* analysis. Various physical phenomena such as gas evolution, cracking and so on which could be only identified using electrochemical measurements can be discriminated using AE [3–9]. Quite recently, we have reported that the AE technique was useful for the *in situ* analysis of physical phenomena linked to electrochemical processes occurring at a $MmNi_{3.6}Mn_{0.4}Al_{0.3}Co_{0.7}$ alloy negative electrode during first charging, including the cracking of alloy particles and hydrogen evolution [10]. In the present study, we will characterize the initial activation behaviors for two kinds of alloy electrodes by *in situ* monitoring with the AE technique.

2. Experimental

Ingots of $MmNi_{3.6}Mn_{0.4}Al_{0.3}Co_{0.7}$ (Mm: Mischmetal) and $TiCr_{0.3}V_{1.8}Ni_{0.3}$ alloys were prepared by an arc melting method in an Ar atmosphere. Mischmetal

* Corresponding author. Tel.: +81 72 254 9283; fax: +81 72 254 9283.
E-mail address: inoue-h@chem.osakafu-u.ac.jp (H. Inoue).

0925-8388/$ – see front matter © 2006 Elsevier B.V. All rights reserved.
doi:10.1016/j.jallcom.2006.12.079

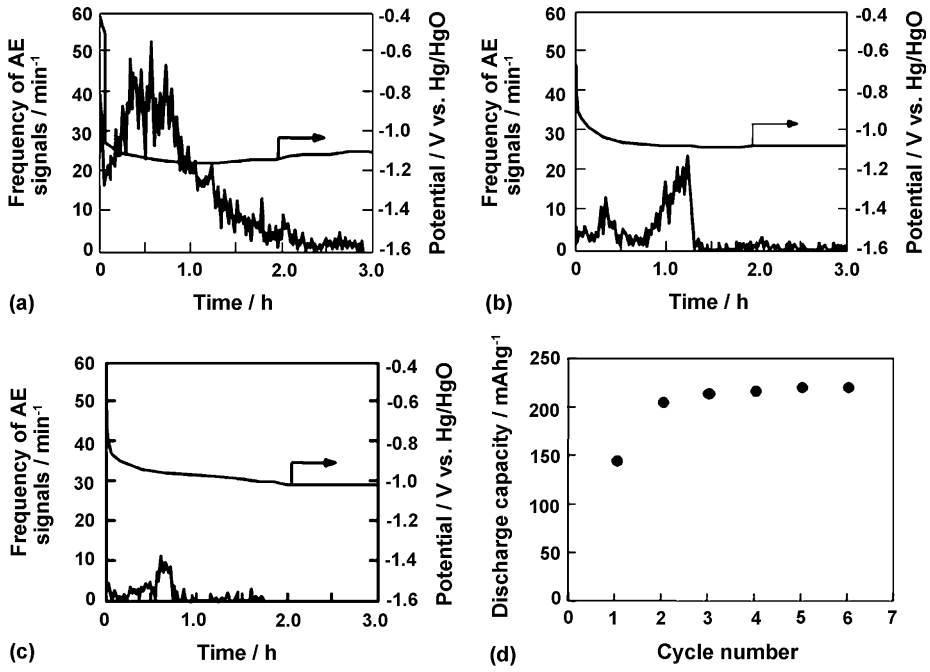

Fig. 1. Time history of frequency of AE signals and electrode potential in (a) first, (b) second and (c) sixth charging processes and (d) initial activation behavior for a $MmNi_{3.6}Mn_{0.4}Al_{0.3}Co_{0.7}$ electrode.

is composed of Ce (55.24 mass%), La (24.19%), Nd (15.08%), Pr (5.43%) and Sm (0.06%). Each alloy ingot was ground into powder and sieved into powders with particle sizes of 106–125 μm for the $MmNi_{3.6}Mn_{0.4}Al_{0.3}Co_{0.7}$ alloy and 75–106 μm for the $TiCr_{0.3}V_{1.8}Ni_{0.3}$ alloy. Each alloy powder was mixed with Cu powder with a mass ratio of 1:3, and the mixture was subjected to a pressure of 200 MPa at room temperature for 1 min yielding pellets for a negative electrode.

An experimental cell assembly for AE monitoring has been shown in the previous paper [10]. The pellet-type negative electrode, a sulfonated-polypropylene separator and a $Ni(OH)_2$/NiOOH positive electrode were stacked. A Ni sheet was inserted between the negative electrode and an AE transducer as a current collector for the negative electrode and a protector of the AE sensor from a 6 M KOH aqueous solution. Before fabricating the cell assembly, the sulfonated-polypropylene separator was thoroughly soaked in a 6 M KOH aqueous solution which was used as the electrolyte. An Hg/HgO electrode was used as a reference electrode.

The $MmNi_{3.6}Mn_{0.4}Al_{0.3}Co_{0.7}$ electrodes were charged at 100 mA g(alloy)$^{-1}$ for 3 h and discharged at 50 mA g(alloy)$^{-1}$ to −0.65 V *versus* Hg/HgO, while the $TiCr_{0.3}V_{1.8}Ni_{0.3}$ electrodes were charged at 100 mA g(alloy)$^{-1}$ for 6 h and discharged at 50 mA g(alloy)$^{-1}$ to −0.75 V *versus* Hg/HgO. In both cases the circuit was opened for 10 min after every charging.

AE monitoring was carried out using an automatic AE monitoring system (NF Electronic Instruments, 7600/0710). An AE transducer (NF electronic Instruments, AE-900S-WB) and a preamplifier (30 dB gain for the $MmNi_{3.6}Mn_{0.4}Al_{0.3}Co_{0.7}$ particles and 40 dB gain for the $TiCr_{0.3}V_{1.8}Ni_{0.3}$ particles) were used in the present study. The elastic waves generated by various phenomena such as cracking were detected by the AE transducer and transformed into AE signals. The AE signals were amplified by the preamplifier and stored in the automatic AE monitoring system. The stored data were displayed as time histories, AE waveforms and power spectra of the AE signals. The AE waveforms and power spectra express the duration of the AE signals and distribution of frequencies for the AE signals, respectively.

All experiments were carried out at room temperature. The surface morphology of the alloys before and after various charge–discharge cycles was characterized using a field-emission scanning electron microscope (Hitachi, S-4500).

3. Results and discussion

3.1. The $MmNi_{3.6}Mn_{0.4}Al_{0.3}Co_{0.7}$ electrode

Fig. 1 shows time history of frequency of AE signals and electrode potential in the first, second and sixth charging processes and initial activation behavior for a $MmNi_{3.6}Mn_{0.4}Al_{0.3}Co_{0.7}$ electrode. The frequency is defined as the number of AE signals with amplitude over a threshold of 0.5 V min^{-1} in the present study. The discharge capacity at first cycle was ca. 140 mAh g^{-1} and then increased with the cycle number and reached a constant value at the fourth cycle, indicating the completion of initial activation.

It has been found that cracking of alloy particles was characterized by a burst-type AE waveform with duration shorter than 0.1 ms and large amplitude, and a power spectrum with wide frequency distribution, particularly with some peaks at frequencies more than 0.6 MHz [10]. During charging, hydrogen evolution can also occur on the surface of hydrogen storage alloy negative electrodes as a side reaction and was characterized by the AE waveform with a long duration of over 0.15 ms, and a power spectrum with a relatively narrow frequency distribution of around 0.6 MHz and maximum amplitude at about 0.1 MHz [10]. As has already reported [10], a large number of AE signals observed in the first half of the first charging process came from the cracking based on lattice expansion due to hydrogen absorption, while hydrogen evolution proceeded throughout the charging [10]. Fig. 2 shows scanning electron micrographs showing the surface morphology of the $MmNi_{3.6}Mn_{0.4}Al_{0.3}Co_{0.7}$ electrode before and after first, second and sixth charge–discharge cycles. As can be seen from this

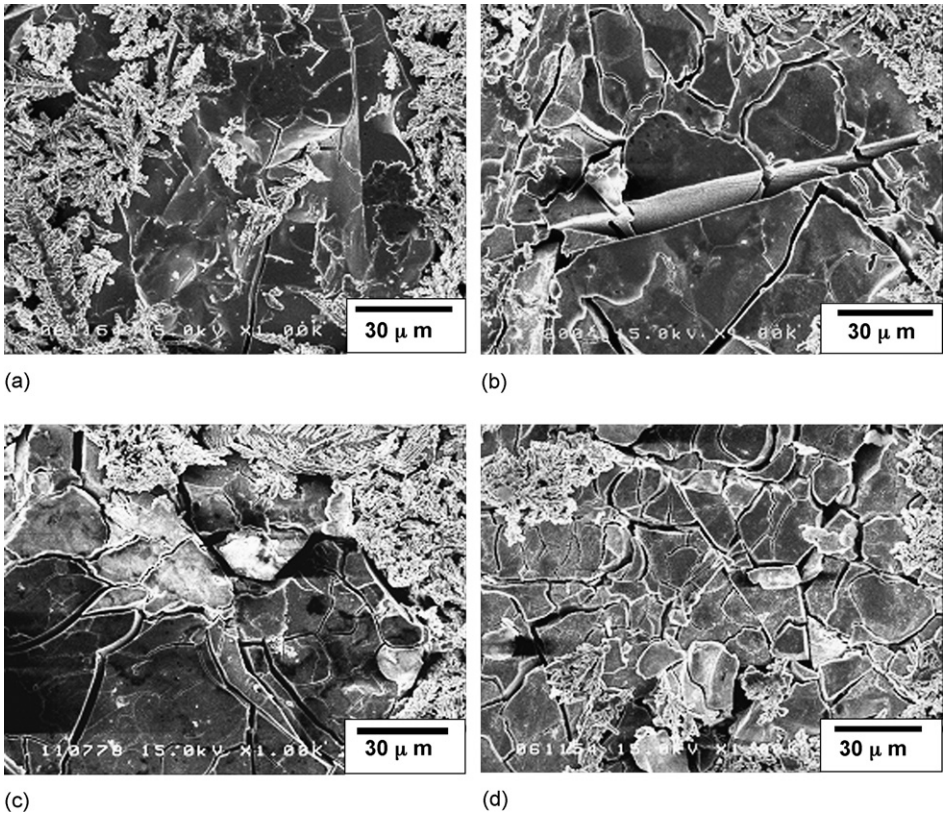

Fig. 2. Scanning electron micrographs showing the surface morphology of a $MmNi_{3.6}Mn_{0.4}Al_{0.3}Co_{0.7}$ electrode (a) before and after (b) first, (c) second and (d) sixth charge–discharge cycles.

figure, a number of large and small cracks appeared on the alloy surface after the first charge–discharge cycle, supporting a large number of AE signals observed in Fig. 1.

In the second charging process, the frequency of AE signals decreased greatly compared to the first charging process as shown in Fig. 1. In this case AE waveforms and power spectra for the $MmNi_{3.6}Mn_{0.4}Al_{0.3}Co_{0.7}$ electrode measured every 1 h are summarized in Fig. 3. The cracking based on hydrogen absorption occurred preferentially after 1 h and 2 h while hydrogen evolution proceeded continuously, suggesting that AE signals observed at around 1 h in the second charging process (see Fig. 1(b)) were ascribed to the cracking of alloy particles. The scanning electron micrograph after second cycle showed that smaller cracks increased compared to after first cycle.

After sixth cycle, the number of AE signals still decreased and discharge capacity showed a constant value as shown in Fig. 1. A lot of finer cracks were observed after sixth cycle as shown in Fig. 2. In this way, *in situ* analysis by the AE technique

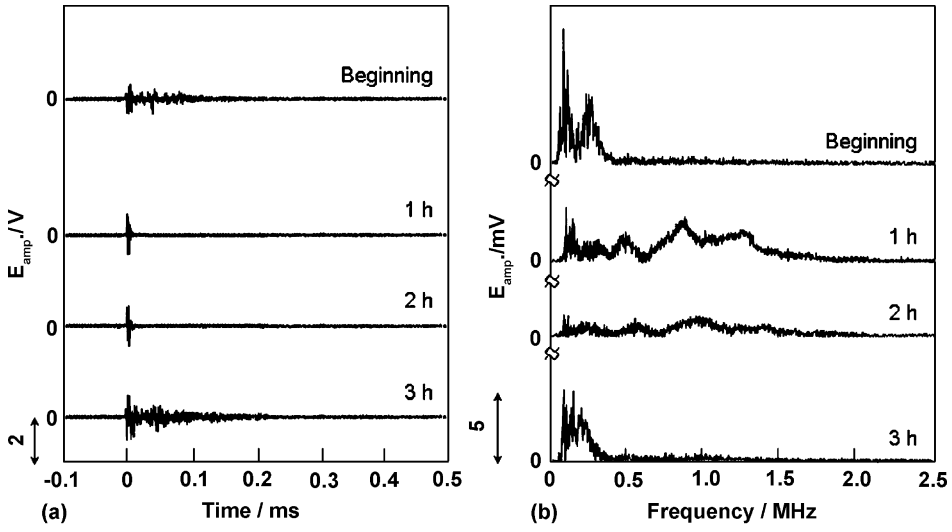

Fig. 3. (a) AE waveforms and (b) power spectra for a $MmNi_{3.6}Mn_{0.4}Al_{0.3}Co_{0.7}$ electrode measured every 1 h during the second charging process.

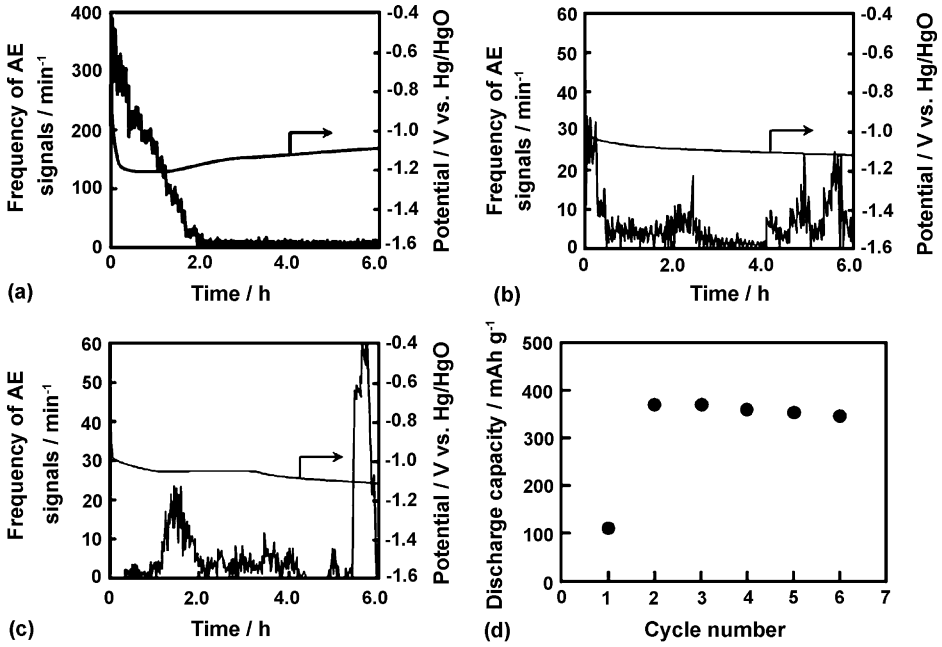

Fig. 4. Time history of frequency of AE signals and electrode potential in (a) first, (b) second and (c) sixth charging processes and (d) initial activation behavior for a $TiCr_{0.3}V_{1.8}Ni_{0.3}$ electrode.

confirms the well-known conclusion that during initial activation the $MmNi_{3.6}Mn_{0.4}Al_{0.3}Co_{0.7}$ particles cracks frequently and the increase in the cracks with cycle number led to the increase in discharge capacity [1].

3.2. The $TiCr_{0.3}V_{1.8}Ni_{0.3}$ electrode

We have found that a $TiV_{2.1}Ni_{0.3}$ alloy, one of V-based alloys, had high discharge capacity of 460 mAh g^{-1} but the discharge capacity became a third of the maximum after 20 charge–discharge cycles, indicating that the $TiV_{2.1}Ni_{0.3}$ electrode had poor cycle durability [11–13]. In our preliminary experiments for improving the cycle durability, we found that the discharge capacity for a $TiCr_{0.3}V_{1.8}Ni_{0.3}$ electrode decreased by only 8% even at 20th cycle, indicating clearly that the $TiCr_{0.3}V_{1.8}Ni_{0.3}$ alloy had much better cycle durability than the $TiV_{2.1}Ni_{0.3}$ alloy. So we investigated time history of frequency of AE signals and electrode potential in first, second and sixth charging processes and initial activation behavior for the $TiCr_{0.3}V_{1.8}Ni_{0.3}$ electrode. The results are summarized in Fig. 4. We raised the gain of a preamplifier in this case because AE signals were weak compared to those for the $MmNi_{3.6}Mn_{0.4}Al_{0.3}Co_{0.7}$ electrode. A large number of AE signals were observed for the first 2 h in the first charging process. Since the electrode potential was −1.2 V *versus* Hg/HgO in this term, hydrogen evolution was expected to proceed preferentially. This seems to suggest that in the beginning of the first charging the alloy surface is covered by oxides of some alloy components

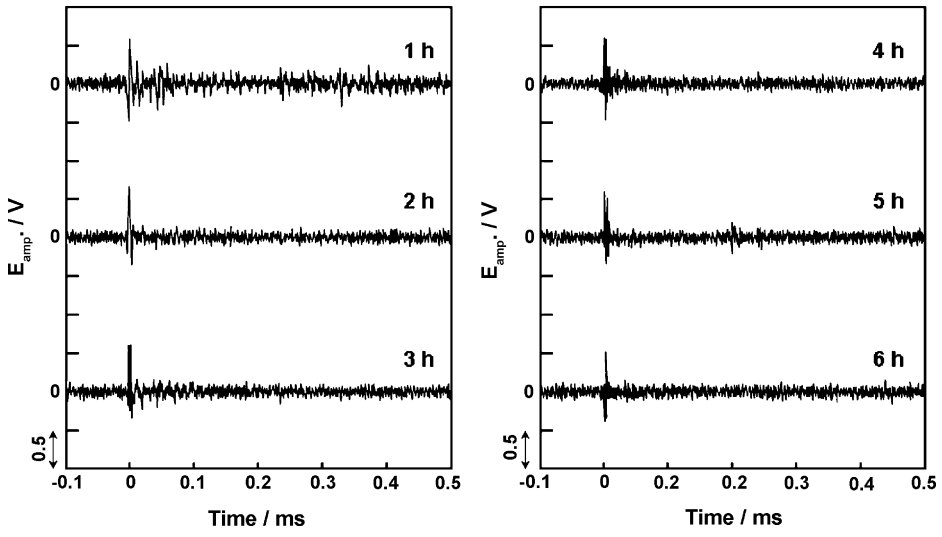

Fig. 5. AE waveforms for a $TiCr_{0.3}V_{1.8}Ni_{0.3}$ electrode measured every 1 h during the first charging process.

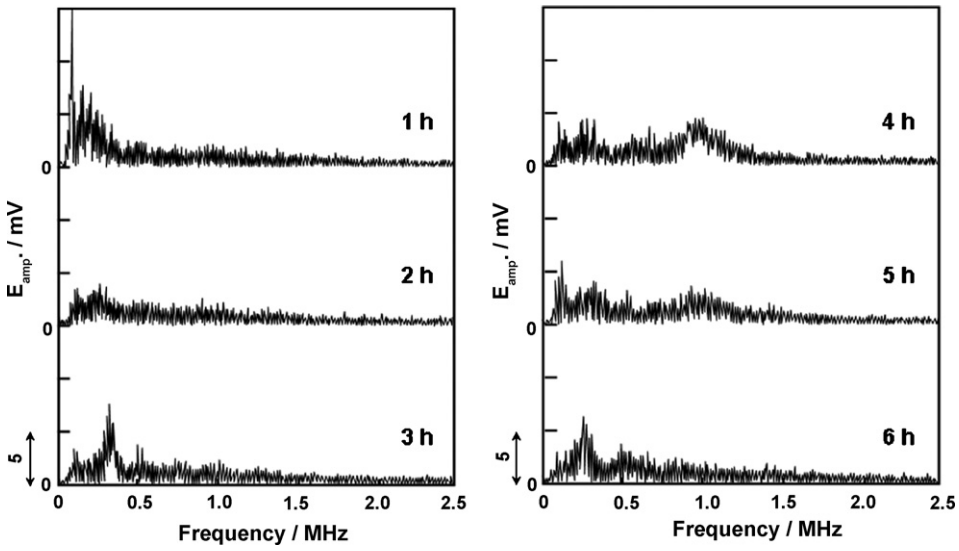

Fig. 6. Power spectra for a $TiCr_{0.3}V_{1.8}Ni_{0.3}$ electrode measured every 1 h during the first charging process.

to inhibit hydrogen absorption in the alloy. Figs. 5 and 6 show AE waveforms and power spectra for the $TiCr_{0.3}V_{1.8}Ni_{0.3}$ electrode measured every 1 h during the first charging process. Both an AE waveform and power spectrum after 1 h exhibit that hydrogen evolution proceeds, supporting the inference from Fig. 4(a). In further charging, an AE waveform and power spectrum identified as the cracking were mainly observed, but the cracking was sporadic as long as we see the time history of the frequency of AE signals. In addition, the $TiCr_{0.3}V_{1.8}Ni_{0.3}$ electrode began to crack later than the $MmNi_{3.6}Mn_{0.4}Al_{0.3}Co_{0.7}$ electrode, suggesting that the former was more patient for cracking than the latter. The maximum amplitude of AE waveforms was just ca. one forth of that for the $MmNi_{3.6}Mn_{0.4}Al_{0.3}Co_{0.7}$ electrode, suggesting that relatively small cracks were formed on the $TiCr_{0.3}V_{1.8}Ni_{0.3}$ alloy surface. From the scanning electron micrograph after first cycle shown in Fig. 7, it was found that a few and relatively small

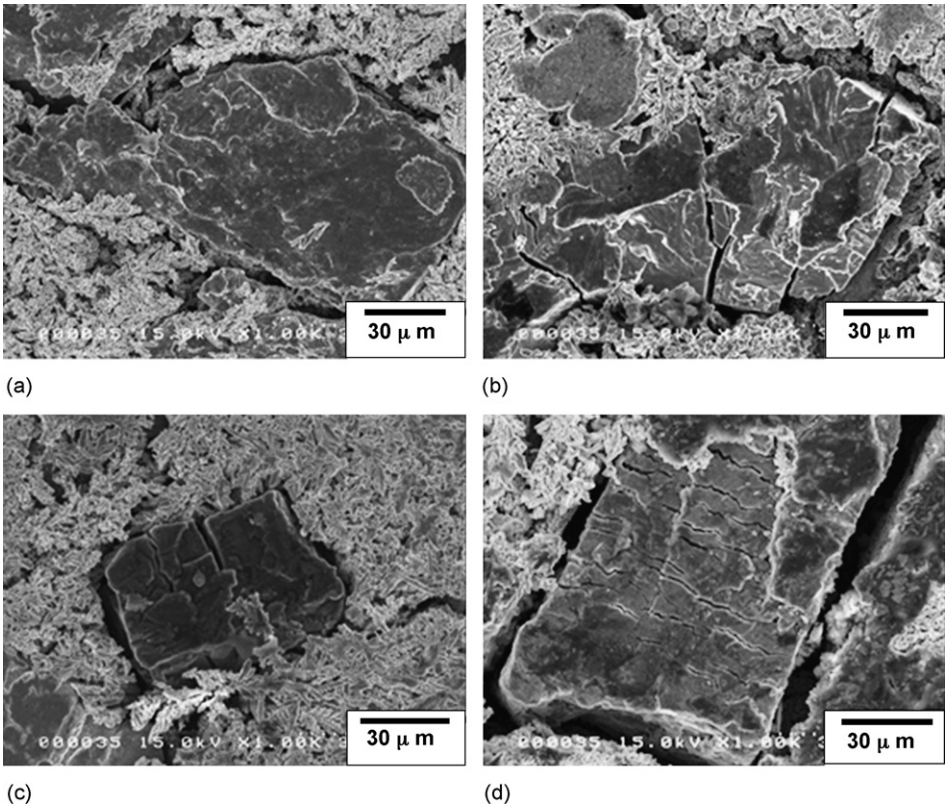

Fig. 7. Scanning electron micrographs showing the surface morphology of a $TiCr_{0.3}V_{1.8}Ni_{0.3}$ electrode (a) before and after (b) first, (c) second and (d) sixth charge–discharge cycles.

cracks were observed on the $TiCr_{0.3}V_{1.8}Ni_{0.3}$ particles, which was with the suggestion from the AE measurements

The frequency of AE signals decreased greatly with repeating charge–discharge cycles as shown in Fig. 4. From the analyses of AE waveforms and power spectra measured every 1 h in the second charging process, it was found that the cracking based on hydrogen absorption was dominant during charging. As can be seen from Fig. 4(d), the discharge capacity for the $TiCr_{0.3}V_{1.8}Ni_{0.3}$ electrode greatly increases in the first 2 cycles, suggesting initial activation. The initial activation seems to be because the surface oxides which inhibited hydrogen absorption into alloy were removed or fresh surface was exposed by sporadic cracking of alloy particles during the first cycle. As a result, hydrogen absorption can occur from the beginning of the second charging. Fig. 7 shows that the $TiCr_{0.3}V_{1.8}Ni_{0.3}$ particles are not pulverized like the $MmNi_{3.6}Mn_{0.4}Al_{0.3}Co_{0.7}$ particles in initial activation, which is characteristic of the $TiCr_{0.3}V_{1.8}Ni_{0.3}$ particles. Nevertheless the $TiCr_{0.3}V_{1.8}Ni_{0.3}$ electrode has higher discharge capacity than the $MmNi_{3.6}Mn_{0.4}Al_{0.3}Co_{0.7}$ electrode and is comparable to the $TiV_{2.1}Ni_{0.3}$ electrode, suggesting that sites occupied by hydrogen in the $TiV_{2.1}Ni_{0.3}$ alloy are kept even in the $TiCr_{0.3}V_{1.8}Ni_{0.3}$ alloy. It seems that the partial substitution with the Cr component does not bring any serious problems on hydrogen diffusion in alloy and electron transfer at electrode surface.

4. Conclusion

We have analyzed initial activation behaviors of $MmNi_{3.6}Mn_{0.4}Al_{0.3}Co_{0.7}$ and $TiCr_{0.3}V_{1.8}Ni_{0.3}$ electrodes using an AE technique in terms of waveforms, power spectra and time history of the AE signals. The $MmNi_{3.6}Mn_{0.4}Al_{0.3}Co_{0.7}$ particles cracked intensively in the first half of the first charging process and were broken down with many large and small cracks during initial activation. In contrast, the $TiCr_{0.3}V_{1.8}Ni_{0.3}$ particles cracked sporadically after hydrogen evolution in the first charging process and the AE signals for the cracking were very weak compared to those for the $MmNi_{3.6}Mn_{0.4}Al_{0.3}Co_{0.7}$ particles.

References

[1] C. Iwakura, H. Inoue, S. Nohara, Encyclopedia of Materials: Science and Technology. Hydrogen–Metal Systems: Electrochemical Reactions (Fundamentals and Applications), Elsevier Science, Amsterdam, 2001, pp. 3923–3941.
[2] P.H.L. Notten, J.L.C. Daams, R.E.F. Einerhand, J. Alloys Compd. 210 (1994) 233.
[3] M. Fregonese, H. Idrissi, H. Mazille, L. Renaud, Y. Cetre, Corros. Sci. 43 (2001) 627.
[4] J. Bernard, M. Boinet, M. Chatenet, F. Dalard, Electrochem. Solid-State Lett. 8 (2005) E53.
[5] K. Darowicki, J. Orlikowski, A. Arutunow, W. Jurczak, Electrochem. Solid-State Lett. 8 (2005) B55.
[6] R. Ramesh, C.K. Mukhopadhyay, T. Jayakumar, B. Raj, Scripta Met. 38 (1998) 661.
[7] S.T. Tsai, H.C. Shih, J. Electrochem. Soc. 145 (1998) 1968.
[8] T. Ohzuku, H. Tomura, K. Sawai, J. Electrochem. Soc. 144 (1997) 3496.
[9] K. Sawai, H. Tomura, T. Ohzuku, Denki Kagaku (currently Electrochemistry) 66 (1998) 301.
[10] H. Inoue, R. Tsuzuki, S. Nohara, C. Iwakura, Electrochem. Solid-State Lett. 9 (2006) A504.
[11] C. Iwakura, W.-K. Choi, R. Miyauchi, H. Inoue, J. Electrochem. Soc. 147 (2000) 2503.
[12] H. Inoue, R. Miyauchi, R. Shin-ya, W.-K. Choi, C. Iwakura, J. Alloys Compd. 330–332 (2002) 597.
[13] H. Inoue, R. Miyauchi, T. Tanaka, W.-K. Choi, R. Shin-ya, J. Murayama, C. Iwakura, J. Alloys Compd. 325 (2001) 299.